Electronic Supplementary Material (ESI) for Nanoscale Horizons.

Supporting Information for:

A plasmon-based nanoruler to probe the mechanical properties of synthetic and biogenic nanosized lipid vesicles

Lucrezia Caselli, Andrea Ridolfi, Jacopo Cardellini, Lewis Sharpnack, Lucia Paolini, Marco Brucale, Francesco Valle, Costanza Montis, Paolo Bergese and Debora Berti

Supplementary Materials and Methods

Materials

Tetrachloroauric (III) acid (≥ 99.9%) and trisodium citrate dihydrate (≥ 99.9%) for the synthesis of AuNPs were provided by Sigma-Aldrich (St. Louis, MO). 1,2-dioleoyl-sn-glycero-3-phosphocholine (DOPC) (>99%), 1-palmitoyl-2-oleoyl-sn-glycero-3-phosphocholine (POPC) (≥ 98.0%), 1,2-dipalmitoyl-sn-glycero-3-phosphocholine (DPPC) (>99%) and 1,2-distearoyl-sn-glycero-3-phosphocholine (DSPC) (>99%) for the liposomes preparation were provided by Sigma-Aldrich (St. Louis, MO). All chemicals were used as received. Milli-Q grade water was used in all preparations.

Synthesis of citrated AuNPs

Anionic gold nanospheres of 16 nm in size were synthesized according to the Turkevich-Frens method [1,2]. Briefly, 20 mL of a 1mM $HAuCl_4$ aqueous solution was brought to boiling temperature under constant and vigorous magnetic

stirring. 2 mL of 1% citric acid solution were then added and the solution was further boiled for 20 minutes, until it acquired a deep red color. The nanoparticles dispersion was then slowly cooled down to room temperature.

Preparation of liposomes

The proper amount of lipid was dissolved in chloroform and a lipid film was obtained by evaporating the solvent under a stream of nitrogen and overnight vacuum drying. The film was then swollen and suspended in warm (50 °C) milliQ-water by vigorous vortex mixing, in order to obtain a final 4 mg/ml lipid concentration. The resultant multilamellar liposomes in water were subjected to 10 freeze-thaw cycles and extruded 10 times through two stacked polycarbonate membranes with 100 nm pore size at room temperature, to obtain unilamellar liposomes with narrow and reproducible size distribution. The filtration was performed with the Extruder (Lipex Biomembranes, Vancouver (Canada)) through Nuclepore membranes.

Preparation of liposomes/AuNPs hybrids

The hybrid samples preparation procedure for Figure 2a of the main text is the following: 20 µL of liposomes (previously diluted to a final lipid concentration of 0.04 mg/ml) or extracellular vesicles were placed inside a 500 µL UV-Vis

plastic cuvette. Then 100 µL of citrated gold nanoparticles ($6.7 \cdot 10^{-9}$ M, see "Synthesis citrated Gold Nanoparticles" and "Supplementary Characterization of Gold Nanoparticles" of SI) were added, in order to have a final concentration (inside the cuvette) of ~$5 \cdot 10^{-11}$ M and of ~$5 \cdot 10^{-9}$ M for liposomes and AuNPs, respectively, and liposomes/AuNPs number ratio of ~1/100. This liposomes/AuNPs number ratio was selected on the basis of our previous publication [3], which highlights that the aggregation of AuNPs on POPC vesicles -and subsequent AuNPs SPR variations- is promoted by low liposomes amounts within the mix. Thus, such a ratio allows for maximizing the liposomes-induced AuNPs SPR spectral shift for an enhanced sensitivity of the plasmon-based nanoruler assay. Then, samples were incubated for 15 minutes, after that the UV-Vis spectra were recorded.

The hybrid samples preparation procedure for Figure 2b of the main text is the following: fixed volumes (768.9 µL) of AuNPs dispersion ($6.7 \cdot 10^{-9}$ M) were added to 20 µL of liposomes (see Table S4 of SI for liposomes concentration), in order to have a final AuNPs/liposomes number ratio of ~8. Samples were incubated for 15 minutes, then placed in glass capillaries of 1 mm diameter and Small-Angle X-Ray profiles acquired.

UV-vis spectroscopy

UV-Vis spectra were measured with a JASCO UV-Vis spectrophotometer.

Small Angle X-ray Scattering

SAXS measurements for the characterization of AuNPs were carried out on a S3-MICRO SAXS/WAXS instrument (HECUS GmbH, Graz, Austria) which consists of a GeniX microfocus X-ray sealed Cu Kα source (Xenocs, Grenoble, France) of 50 W power which provides a detector focused X-ray beam with λ = 0.1542 nm Cu Kα line. The instrument is equipped with two one-dimensional (1D) position sensitive detectors (HECUS 1D-PSD-50 M system). Each detector is 50 mm long (spatial resolution 54 μm/channel, 1024 channels) and covers the SAXS q-range ($0.003 < q < 0.6\,^{\circ}\text{Å}^{-1}$). The temperature was controlled by means of a Peltier TCCS-3 Hecus. The analysis of SAXS curves was carried out using Igor Pro.[4] SAXS measurement on AuNPs aqueous dispersion was carried out in a sealed glass capillary of 1.5 mm diameter. To analyze gold nanospheres' curves we chose a model function with a spherical form factor and a Schulz size distribution:[5], it calculates the scattering for a polydisperse population of spheres with uniform scattering length density. The distribution of radii is a Schulz distribution given by the following equation:

$$f(R) = (z+1)^{z+1} x^{z} \frac{exp[-(z+1)x]}{R_{avg}\Gamma(z+1)}$$

where R_{avg} is the mean radius, $x = R/R_{avg}$ and z is related to the polydispersity. The form factor is normalized by the average particle volume, using the 3rd moment of R:

$$\langle V \rangle = \frac{4\pi}{3}\langle R^{+3} \rangle = \frac{4\pi}{3}\langle R \rangle^{+3}\frac{(z+3)(z+2)}{(z+1)^2}$$

The scattering intensity is:

$$I(q) = \left(\frac{4\pi}{3}\right)^2 N_0 \Delta\rho^2 \int_0^\infty f(R)R^6F^2(qR)dR$$

where N_0 is the total number of particles per unit volume, $F(R)$ is the scattering amplitude for a sphere and $\Delta\rho$ is the difference in scattering length density between the particle and the solvent.

SAXS measurements for the characterization of AuNPs/liposomes hybrids were collected at beamline ID02 at the European Synchrotron Radiation Facility (ESRF, Grenoble, France) [6]. A scattering vector (of magnitude q) range of $0.007 \leq q \leq 0.2$ nm^{-1} was covered with two sample–detector distances (1 and 10 m) and a single-beam setting for an X-ray monochromatic radiation wavelength with a wavelength of $\lambda = 0.10$ nm (12.46 keV). The beam diameter was adjusted to 72.4 μm in the horizontal (x) direction and 42.3 μm in the vertical (y) direction (full width at half-maximum at the sample). Assuming a Gaussian distribution, the portion of the beam that is hitting outside the channel can be estimated. When the channel is centered, this is ~0.3% but closer to the edge and more beam overlaps the edge. The beamstop diameter was 2 mm. As a detector, a 2D Rayonix MX-

170HS with a pixel size of 44 × 44 μm2 was used, which was housed in an evacuated flight tube, at a sample-to-detector distance of alternatively 10 m (leading to an available q-range of 0.007-0.02 nm^{-1}) or 1 m (leading to an available q-range of 0.07-0.2 nm^{-1}). The exposure times for the background- and sample measurements were 0.5 s for the case of 1 m sample-to-detector distance and 0.3 s for the case of 10 m sample-to-detector distance. Measured scattering patterns were normalized to an absolute intensity scale after applying standard detector corrections and then azimuthally averaged to obtain the one-dimensional intensity profiles, denoted by I (q).

Atomic Force Microscopy (AFM)

Surface Preparation and Sample Deposition

All AFM experiments were performed on poly-L-lysine (PLL) coated glass coverslips. All reagents were acquired from Sigma-Aldrich Inc (www.sigmaaldrich.com) unless otherwise stated. Microscopy borosilicate glass slides (15mm diameter round coverslips, Menzel Gläser) were first immersed in a 3:1 mixture of 96% H_2SO_4 and 50% aqueous H_2O_2 ('oxidising piranha') solution for 2 h in order to remove any organic residue present on their surface; after that, they were cleaned in a sonicator bath (Elmasonic Elma S30H) for 30 minutes in acetone, followed by 30 minutes in isopropanol and 30 minutes in ultrapure water (Millipore Simplicity UV). Clean slides were incubated overnight

in a 0.0001% (w/v) PLL solution at room temperature, thoroughly rinsed with ultrapure water and dried with nitrogen. A 10 µl-droplet of the vesicle-containing solution under study was deposited on a PLL-functionalized glass slide and left to adsorb for 10 minutes at 4°C, then inserted in the AFM fluid cell (see below) without further rinsing. The concentration of each vesicle-containing solution was adjusted in order to maximize the surface density of isolated, individual vesicles and minimize clusters of adjoining vesicles.

AFM Setup

All AFM experiments were performed in ultrapure water at room temperature on a Bruker Multimode (equipped with Nanoscope V electronics, a sealed fluid cell and a type JV piezoelectric scanner) using Bruker SNL-A probes (triangular cantilever, nominal tip curvature radius 2-12 nm, nominal elastic constant 0.35 N/m, calibrated with the thermal noise method.

AFM Imaging

Imaging was performed in PeakForce mode. In order to minimize vesicle deformation or rupture upon interaction with the probe, the applied force setpoint was kept in the 150-250 pN range. Lateral probe velocity was not allowed to exceed 5µm/s. Feedback gain was set at higher values than those usually employed for optimal image quality in order to ensure minimal probe-induced vesicle deformation upon lateral contact along the fast scan axis (please refer to Ridolfi et al. [7] for further details). The average height value of all bare substrate

zones was taken as the baseline zero height reference. Image background subtraction was performed using Gwyddion 2.53.16 [8].

AFM-based Force Spectroscopy (AFM-FS)

The mechanical characterization of vesicles via AFM force spectroscopy was performed by first scanning the sample (see previous paragraph) to locate individual vesicles. The chosen vesicles were then imaged reducing the scan size for achieving higher accuracy. We recorded a series of force/distance curves at multiple XY positions (typically around 64-100 curves arranged in a square array covering the vesicle initial location) for each individual vesicle. In most cases, only a few curves showed the mechanical fingerprint of an intact vesicle response to indentation: a linear deformation upon applied pressure during probe penetration. Of these, we first discarded those curves with probe-vesicle contact points occurring at probe-surface distances below vesicle height as measured by imaging. Remaining traces (typically 1-3 per vesicle) were analyzed to calculate vesicle stiffness (k_S).

Transmission Electron Microscopy

Trasmission electron microscopy (TEM) images were acquired with a STEM CM12 Philips electron microscope equipped with an OLYMPUS Megaview G2 camera, at CeME (CNR Florence Research Area, Via Madonna del Piano, 10 - 50019 Sesto Fiorentino). A drop of citrated AuNPs, diluted ten times, was placed

on 200 mesh carbon-coated copper grids with a diameter of 3 mm and a thickness of 50 μm (Agar Scientific) and dried at room temperature. Then, the sample was analyzed at an accelerating voltage of 100 keV.

Dynamic Light Scattering

DLS measurements at $\theta = 90°$ were performed using a Brookhaven Instrument 90 Plus (Brookhaven, Holtsville, NY). Each measurement was an average of ten repetitions of one minute each and repeated ten times. The autocorrelation functions were analyzed through the cumulant fitting stopped to the second order or with Laplace inversion according to CONTIN algorithm, allowing an estimate of the hydrodynamic diameter of particles.

Z-Potential Measurements

Zeta potential measurements were performed using a Zeta Potential Analyzer (Zeta Plus, Brookhaven Instruments Corporation, Holtsville, NY). Zeta potentials were obtained from the electrophoretic mobility u, according to Helmholtz-Smoluchowski equation: $\zeta = (\eta/\varepsilon) \times u$ with η being the viscosity of the medium, ε the dielectric permittivity of the dispersing medium. The Zeta Potential values are reported as averages from ten measurements.

Supplementary Characterization of Gold Nanoparticles

Transmission Electron Microscopy

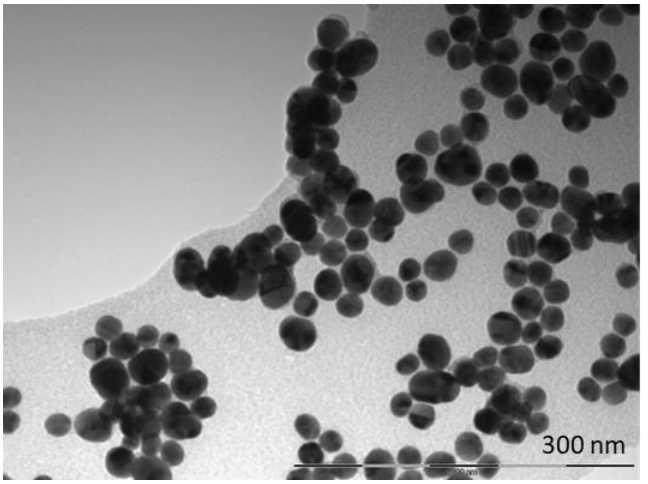

Figure S1 Representative Transmission electron microscopy (TEM) images of citrated gold nanoparticles acquired with a STEM CM12 Philips electron microscope, at CeME (CNR Florence Research Area, Via Madonna del Piano, 10 - 50019 Sesto Fiorentino). The sample was placed on a 200 mesh carbon-coated copper grid.

Small Angle X-ray Scattering

The analysis of SAXS curves was carried out using Igor Pro.[4] SAXS measurements on AuNPs aqueous dispersion were carried out in sealed glass capillaries of 1.5 mm diameter. To analyze gold nanospheres' curves we chose a model function with a spherical form factor and a Schulz size distribution:[5], it calculates the scattering for a polydisperse population of spheres with uniform scattering length density. The distribution of radii is a Schulz distribution given by the following equation:

$$f(R) = (z+1)^{z+1} x^z \frac{exp[-(z+1)x]}{R_{avg}\Gamma(z+1)}$$

where R_{avg} is the mean radius, $x = R/R_{avg}$ and z is related to the polydispersity. The form factor is normalized by the average particle volume, using the 3rd moment of R:

$$\langle V \rangle = \frac{4\pi}{3}\langle R^{+3} \rangle = \frac{4\pi}{3}\langle R \rangle^{+3} \frac{(z+3)(z+2)}{(z+1)^2}$$

The scattering intensity is:

$$I(q) = \left(\frac{4\pi}{3}\right)^2 N_0 \Delta\rho^2 \int_0^\infty f(R) R^6 F^2(qR) dR$$

where N_0 is the total number of particles per unit volume, $F(R)$ is the scattering amplitude for a sphere and $\Delta\rho$ is the difference in scattering length density between the particle and the solvent. The structural parameters (Table S1) of citrated gold nanoparticles were evaluated from the SAXS profile of their water dispersion (Figure S2) according to the models reported in the Materials and Methods section of SI.

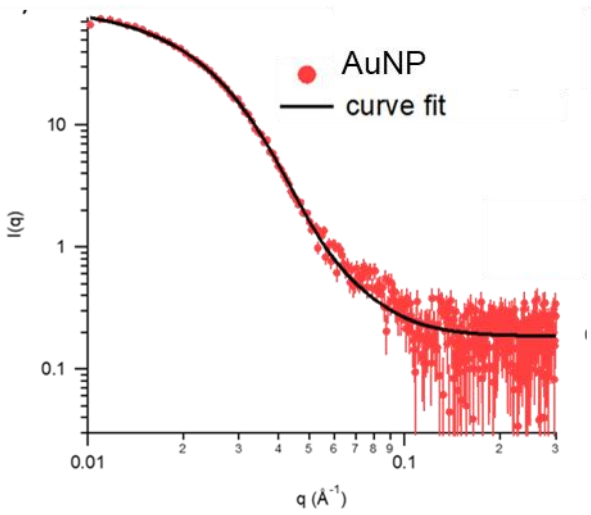

Figure S2 Experimental SAXS curve (red markers) obtained for AuNPs and curve fit (solid black line) according to the Schulz spheres model from the NIST package SANS Utilities. The size and polydispersity obtained from the fitting procedure are summarized in the Table S1 below.

	R_{core} (nm)	poly
AuNP	6.5	0.3

Table S1 Structural parameters of the nanoparticles obtained from the analysis of SAXS curves according to the the Schulz spheres model.

Dynamic Light Scattering and Z-Potential

AuNPs hydrodynamic diameter and surface charge in MilliQ water were evaluated through Dynamic Light Scattering and Zeta-Potential, respectively,

and reported in Table S2.

	D_h (nm)	Z-Potential (mV)
AuNPs	15.8 ± 0.3	-36 ± 2

Table S2 Hydrodynamic diameter obtained from Dynamic Light Scattering and Zeta Potential values of AuNPs.

UV-vis Spectroscopy

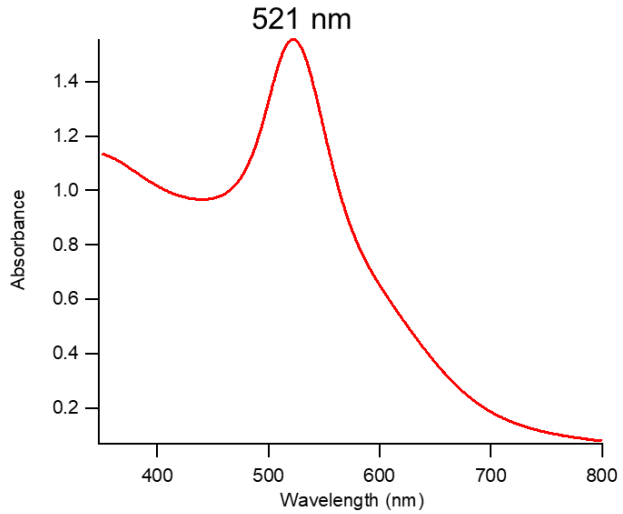

Figure S3 UV-Vis absorption spectra of AuNPs after 1:5 dilution in water. The plasmon absorption peak is at around 521 nm.

The size of AuNPs was further evaluated from UV-Vis Spectroscopy by the following equation [9]:

$$d = \exp\left(B_1 \frac{A_{spr}}{A_{450}} - B_2\right)$$

with d diameter of gold nanoparticles, A_{spr} absorbance at the surface plasma resonance peak, A_{450} absorbance at the wavelength of 450 nm and B_1 and B_2 are dimensionless parameters, taken as 3 and 2.2, respectively. The diameter value obtained is of 13.5 nm.

The concentration of citrated gold nanoparticles was determined via UV-Vis spectrometry, using the Lambert-Beer law ($E(\lambda) = \varepsilon(\lambda)lc$), taking the extinction values $E(\lambda)$ at the LSPR maximum, i.e. λ = 521 nm. The extinction coefficient $\varepsilon(\lambda)$ of gold nanoparticles dispersion was determined by the method reported in literature [10], by the following equation:

$$\ln(\varepsilon) = k\ln(d) + a$$

with d core diameter of nanoparticles, and k and a dimensionless parameters ($k = 3.32111$ and $a = 10.80505$). The arithmetic mean of the sizes obtained by optical and scattering analyses was selected, leading to a $\varepsilon(\lambda)$ of $2.8 \cdot 10^8$ $M^{-1}cm^{-1}$. The final concentration of the citrated AuNPs is therefore ~$5.6 \cdot 10^{-9}$ M.

Supplementary Characterization of Liposomes

Dynamic Light Scattering and Zeta-Potential

	D_h (nm)	Zeta P
DOPC	118.6 ± 0.2	-16 ± 1
POPC	103.8 ± 0.1	-19 ± 3
POPC/DPPC	92.1 ± 0.2	-22 ± 1
DPPC	115.7 ± 0.1	-13 ± 1
DPPC/DSPC	104 ± 0.2	-10 ± 1
DSPC	127.7 ± 0.2	-19 ± 1

Table S3 Hydrodynamic diameter obtained from Dynamic Light Scattering and Zeta Potential values of synthetic liposomes.

Evaluation of Liposomes concentration

The lipid concentration in the starting colloidal dispersion was estimated to be 4 mg/mL from the initial lipid and water amounts employed in the formation and swelling of lipid films (see "Preparation of liposomes" in the Materials and Methods section), assuming the absence of lipid loss due to the extrusion procedure. The liposomes concentration in the final dispersion was subsequently

calculated considering the hydrodynamic diameter of each liposomal batch (Table S3 of SI). In particular, from the liposomes' average diameter, the liposomal surface area (surface area=$4\pi r^2$) can be calculated; the doubled surface can be subsequently divided by the lipid cross section (0.5 nm^2) in order to obtain the lipid number per liposome, assuming that approximately one half of the lipids is localized in the external leaflet of a liposomes, since the bilayer thickness, about 4-5 nm, is negligible with respect to the liposomes' average diameter. Eventually, the total weighted lipid concentration was divided by the total number of lipids per liposome, yielding the real liposome concentration, which is reported in Table S4 for each liposomes' dispersion.

	Concentration (M)
DOPC	$3.2 \cdot 10^{-8}$
POPC	$3.1 \cdot 10^{-8}$
POPC/DPPC	$3.6 \cdot 10^{-8}$
DPPC	$3.1 \cdot 10^{-8}$
DPPC/DSPC	$3.8 \cdot 10^{-8}$
DSPC	$3.5 \cdot 10^{-8}$

Table S4 Final liposomes' concentration in each liposomal batch.

Supplementary Characterization of EVs

Zeta Potential

The Zeta Potential of EVs dispersion in milliQ water was measured as described in the "Material and Methods" section of SI and is equal to -21 ± 3 mV.

AFM characterization of synthetic and natural lipid vesicles

AFM Mechanical Characterization

According to the Canham-Helfrich theory, the mechanical response of a vesicle to an applied force is elastic; this behavior is reflected in the linear relationship between the force and tip penetration, in the AFM force-distance curves, right after the contact point (see Fig.1b in the main text). Calculating the slope of this linear part, gives the value of the vesicle stiffness, a mechanical parameter that accounts for multiple contributions, the most relevant being the intrinsic membrane rigidity (the bending modulus) and the vesicle luminal, i.e. internal, pressure. The latter contribution describes the vesicle pressurization following the deformation applied by the AFM tip. This deformation generates a volume variation that increases the pressure within the vesicle. While the bending modulus is an intrinsic descriptor of the lipid membrane bending rigidity, the internal pressure and hence the stiffness depend on the size of each vesicle. Indeed, the volume variation associated with a given tip penetration varies with

the vesicle size (i.e. the same penetration will result in higher volume variations for smaller vesicles); as a consequence, vesicles that are heterogenous in size will be subjected to different pressurizations following similar indentation events. However, both the measured liposomes and EVs are characterized by low polydispersity, this allows considering the stiffness a size-independent parameter. Moreover, since all the tested liposomes were characterized by similar size distributions and same polar headgroups, they will experience similar pressurizations and electrostatic attractions to the substrate; as a result, we can assume that changes in their stiffness are entirely ascribable to differences in their membrane rigidity, which can be recapitulated by the bending modulus. Membrane rigidity may vary depending on the phase behavior of the lipid bilayer, a temperature dependent parameter. All the measurements were performed at 28°C, where neat DOPC and POPC vesicles are in the fluid phase, while DPPC and DSPC ones are in the gel phase. In fluid-state membranes, lipid molecules can diffuse freely within the bilayer plane, while in gel- state membranes lipids are more tightly packed and their motion is more constrained. As a consequence, gel- phase bilayers are expected to be stiffer than fluid- phase ones. Our results from the Force Spectroscopy FS analysis (Figure 1c, main text) confirms this behavior, with DPPC and DSPC vesicles being substantially stiffer than DOPC and POPC ones. Two other important parameters that can affect the stiffness of a lipid bilayer are the chain length and its degree of saturation; e. g. DSPC

possesses two fully saturated chains, longer than all the other measured ones, resulting in the highest measured stiffness. Overall, the obtained stiffness values for neat DOPC, POPC, DPPC and DSPC vesicles (Figure 1c, main text) are in good agreement with results from recent AFM-FS investigations on similar vesicles [11]. Another interesting aspect to highlight is that the stiffnesses measured for the hybrid lipid vesicles (POPC/DPPC and DPPC/DSPC) have intermediate values with respect to liposomes made of the two pure components.

AFM-based characterization of EVs size distribution, concentration and purity

AFM imaging was employed to obtain the size distribution of the EVs sample. A total of 166 EVs were imaged; from the topography of the AFM images, assuming the vesicle surface area conservation and by applying simple geometric consideration (see Ridolfi et al.[12] for further details) it is possible to obtain the values of the diameter that the vesicles would have had in solution, prior to their adsorption to the surface (we refer to this parameter as "Size"). Figure S4 displays the size distribution for the EVs sample used in this study. The measured EVs have a mean size of 74 nm with a standard deviation of 30 nm.

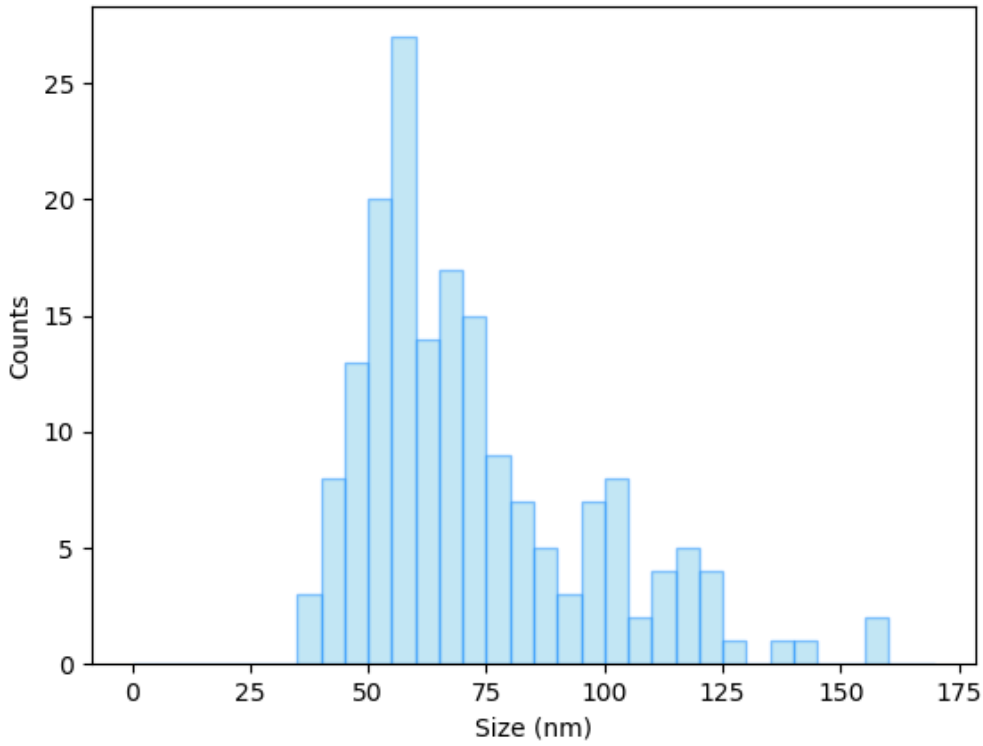

Figure S4: EVs size distribution obtained from the AFM imaging analysis. The size of the EVs (reported in the horizontal axis), indicates the diameter that the vesicles would have had in solution, prior to their adsorption.

Exploiting the AFM-based characterization method developed by Ridolfi et al.[7], it is also possible to detect the presence of contaminants that, from a physico-chemical point of view, do not behave like a lipid vesicle; the method is based on the calculation of the contact angle (CA) that each vesicle displays after adsorption on the surface. Both synthetic lipid vesicles and EVs are characterized by a narrow distribution of CA over the whole range of characteristic sizes. Figure S5 shows the CA values of each of the imaged EVs, plotted against their

size; as can be seen, the scatterplot displays only the fingerprint of the typical vesicle-like behavior, ruling out the presence of any contaminant on the surface.

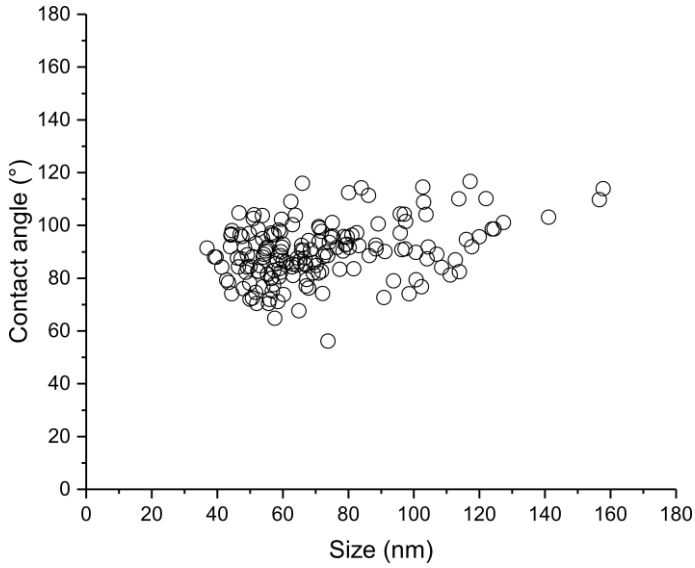

Figure S5: Scatterplot showing the contact angle of each EV, plotted against their respective size. According to this characterization, the EVs show the typical vesicle-like behavior, i.e. narrow CA distribution over the entire range of sizes (average CA value is 90° and the standard deviation is 11°); pointing to the absence of any spherical contaminant.

AFM imaging was also used to estimate the starting concentration of the EVs sample. To do this, we compared the number of DPPC liposomes (coming from a solution with a known concentration and having a size distribution similar to the EVs) adsorbed on the glass surface with the number of EVs adsorbed on the same glass surface. This represents only a qualitative procedure and it is based on different assumptions: i) the interactions of DPPC liposomes with the glass surface are similar to the EVs ones, ii) the recorded images are representative of both the vesicles samples, iii) the size distributions of the two samples are

similar to each other. The concentration of the DPPC starting solution is 0.02 mg/ml; analysing the AFM images, we recorded a total of 329 vesicles in 4 different images, giving an average of 82.25 vesicles per image. Measuring EVs from TRAMP cells, we sampled 5 images, obtaining a total number of 166 EVs; 33.20 EVs per image. From proportionality considerations, it is possible to estimate the concentration of the EVs, spotted on the glass coverslips, using the following expression:

DPPC concentration (mg/ml):DPPC liposomes per image=EVs concentration (mg/ml) :EVs per image

From the expression we obtained a concentration of 0.008 mg/ml for the EVs sample. Since the EVs starting solution have been diluted six times before being spotted on the glass surface, the starting concentration is~0.048 mg/ml.

Supplementary Characterization of liposomes/AuNPs hybrids

Small-Angle X-Ray Scattering

SAXS measurements on liposomes/AuNPs hybrids were recorded at ID02 beamline, ESRF (Grenoble, France), using a sample-to-detector distance of 10 m. The analysis of SAXS curves was carried out using Igor Pro[4]. SAXS measurements on liposomes/AuNPs aqueous dispersion were carried out in

sealed glass capillaries of 1 mm diameter.

The SAXS profiles of DOPC liposomes/AuNPs and POPC liposomes/AuNPs in Figure 2b were fitted according to a linear fit in the 0.0695-0.1142 nm^{-1}q-range, to obtain the slope values reported in the main text (-1.5404 ± 0.00297 for DOPC and -1.4987 ± 0.00612 for POPC). The fitting yielded a chisquare of 0.000239052 and 0.00106975, for DOPC/AuNPs and POPC/AuNPs respectively.

The SAXS results of inset of Figure 2b were collected at ID02 beamline, ESRF (Grenoble, France), using a sample-to-detector distance of 1 m.

The scattering intensity (I(q)) is defined by the following equation:

$$I(q) = KN_pV_p^2(\Delta\rho)^2P(q)S(q) + B$$

With k instrumental constant, N_p scattering nanoparticles' number per unit volume, V_p nanoparticle's volume, $\Delta\rho$ contrast of the experiment, B background intensity, P(q) e S(q) form and structure factors, respectively.

In order to obtain the structure factor of the liposome/AuNPs complex, we divided the scattering intensity of the liposomes/AuNPs hybrid by the scattering intensity of the neat AuNPs dispersion (at a suitable dilution of 1:10):

$$\frac{I(q)_{Hyb}}{I(q)_{NP}} \sim \frac{S(q)_{Hyb}P(q)_{Hyb}}{S(q)_{NP}P(q)_{NP}}$$

For a diluted AuNPs dispersion the structure factor can be considered equal to 1. In addition, in the high-q region (0.1-1.6 nm^{-1}), the form factor of

liposomes/AuNP hybrids can be approximated to the one of neat AuNPs, leading to the following:

$$\frac{I(q)_{Hyb}}{I(q)_{NP}} = S(q)_{Hyb}$$

The mean interparticle distance between the AuNPs within the aggregates (d) can be obtained from the S(q) vs q (nm^{-1}) plot (see inset of Figure 2b of the main text), by the following equation:

$$d = \frac{2\pi}{qmax}$$

With q_{max} q value corresponding to the maximum of the correlation peaks reported in the inset of figure 2b (main text).

UV-Vis Spectroscopy

The S.I. mean values for each liposomes/AuNPs mixtures are reported in Table S5, together with the relative standard deviation obtained from five repeated measurements on different samples (see "Preparation of liposomes/AuNPs hybrids" of SI).

	S.I. mean value	Standard deviation
DOPC	1.456	0.002
POPC	1.438	0.001
POPC/DPPC	1.377	0.005
DPPC	1.16	0.01
DPPC/DSPC	1.127	0.003

DSPC	1.026	0.006

Table S5 S.I. mean value and standard deviation for each liposomes/AuNPs hybrid.

The fitting parameters describing the sigmoidal best fit (eqn. 1 of the main text) for the S.I. values of liposomes plotted versus the AFM-determined stiffness, reported in Figure 3b of the main text, are the following:

a	**b**	**c**	**d**	**Chi square**
1.4831 ± 0.0485	-0.51151 ± 0.131	0.026043 ± 0.00266	0.0063004 ± 0.00265	0.0015

Table S6 Fitting parameters obtained by fitting the S.I. vs stiffness values of Figure 3c (main text) through the sigmoidal best fit (refer eqn 1 of main text for description of parameters).

The extent of AuNPs aggregation was also evaluated using different optical indexes, both taken from literature and defined in our lab.

In particular, as an alternative to the bending index defined in the main text, which is based on the determination of the area under the absorbance curve associated to AuNP aggregation, we defined another optical parameter (S.I. (2)). This alternative bending index allows evaluating AuNPs aggregation extent by calculating the intensity difference between the free AuNPs primary plasmon band (at 521 nm) and the aggregated AuNPs secondary plasmon peak, whose maximum is located at about 625 nm (see Figure S6). This result is then divided by the wavelength interval ($\Delta\lambda$) between the two peaks and normalized for the S.I. of neat AuNPs.

$$S.I.(2) = \frac{I_{625} - I_{521}}{\Delta\lambda}$$

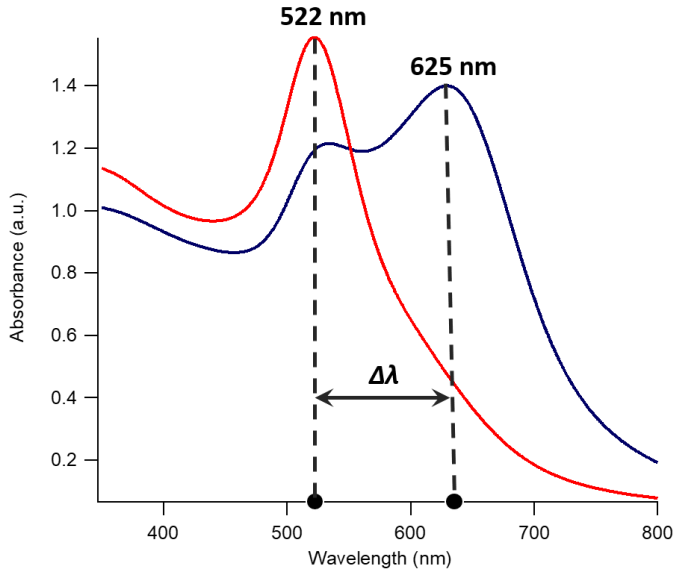

Figure S6 Visual description of the S.I. (2) evaluation.

We also selected another optical index from literature ($A.I._{CONAN}$) [13,14], which is commonly used to describe the aggregation of AuNPs on natural and synthetic vesicles and defined as follows:

$$A.I._{CONAN} = \frac{I_{521}}{I_{650} + I_{800}}$$

with I_{521} , I_{650} and I_{800} UV-Vis absorbances at 521, 650 and 800 nm respectively.

Both the S.I. (2) and the $A.I._{CONAN}$ show a sigmoidal behaviour as a function of membrane stiffness, as reported in Figure S7 and Table S7.

	S.I. (2)	A.I. CONAN
DOPC	-0.1965 ± 0.0004	0.785 ± 0.014
POPC	- 0.14 ± 0.03	0.83 ± 0.17
POPC/DPPC	0.12 ± 0.03	1.02 ± 0.05
DPPC	0.71 ± 0.06	1.99 ± 0.24
DPPC/DSPC	0.76 ± 0.01	2.36 ± 0.05
DSPC	1.04 ± 0.02	3.28 ± 0.24

Table S7 S.I. (2) and A.I. CONAN mean values and standard deviations for each liposomes/AuNPs hybrid.

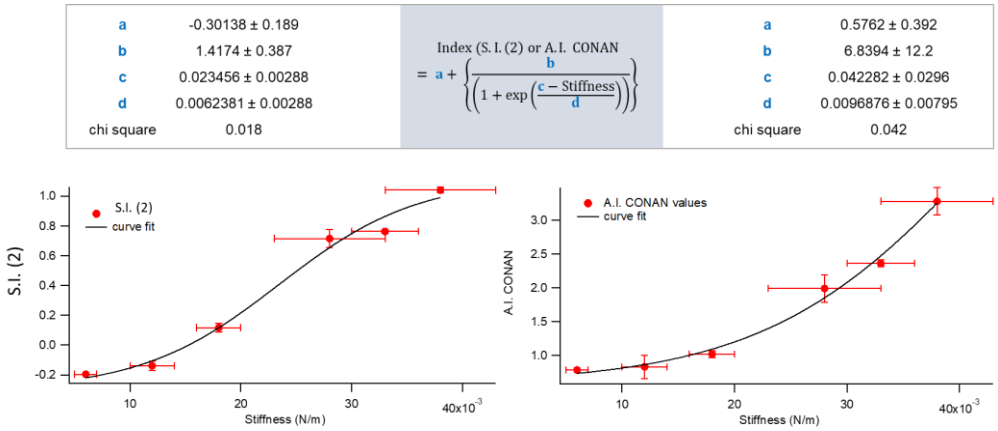

Figure S7 S.I. (2) and A.I. CONAN mean values and as a function of membrane stiffness. The sigmoidal fit curve is shown in black, together with the corresponding equation and fitting parameters (top inset).

Bibliography

1 J. Turkevich, P. C. Stevenson and J. Hillier, *Discuss. Faraday Soc.*, 1951, **11**, 55–75.

2 G. Frens, *Nat. Phys. Sci.*, 1973, **241**, 20–22.

3 C. Montis, L. Caselli, F. Valle, A. Zendrini, F. Carlà, R. Schweins, M. Maccarini, P. Bergese and D. Berti, *J. Colloid Interface Sci.*, 2020, **573**, 204–214.

4 S. R. Kline, *J. Appl. Crystallogr.*, 2006, **39**, 895–900.

5 M. Kotlarchyk and S.-H. Chen, *J. Chem. Phys.*, 1983, **79**, 2461.

6 T. Narayanan, M. Sztucki, P. Van Vaerenbergh, J. Gorini, L. Claustre, F. Sever and J. Morse, *J. Appl. Crystallogr.*, 2018, **51**, 1511–1524.

7 A. Ridolfi, M. Brucale, C. Montis, L. Caselli, L. Paolini, A. Borup, A. T. Boysen, F. Loria, M. J. C. Van Herwijnen, M. Kleinjan, P. Nejsum, N. Zarovni, M. H. M. Wauben, D. Berti, P. Bergese and F. Valle, *Anal. Chem.*, 2020, **92**, 10274–10282.

8 D. Nečas and P. Klapetek, *Cent. Eur. J. Phys.*, 2012, **10**, 181–188.

9 W. Haiss, N. T. K. Thanh, J. Aveyard and D. G. Fernig, *Anal. Chem.*, 2007, **79**, 4215–4221.

10 X. Liu, M. Atwater, J. Wang and Q. Huo, *Colloids Surfaces B Biointerfaces*, 2007, **58**, 3–7.

11 D. Vorselen, F. C. Mackintosh, W. H. Roos and G. J. L. Wuite, *ACS Nano*, 2017, **11**, 2628–2636.

12 A. Ridolfi, M. Brucale, C. Montis, L. Caselli, L. Paolini, A. Borup, A. T. Boysen, F. Loria, M. J. C. van Herwijnen, M. Kleinjan, P. Nejsum, N. Zarovni, M. H. M. Wauben, D. Berti, P. Bergese and F. Valle, *Anal. Chem.*, 2020, **92**, 10274–10282.

13 S. Busatto, A. Giacomini, C. Montis, R. Ronca and P. Bergese, *Anal. Chem.*, 2018, **90**, 7855–7861.

14 R. Carney, A. Zendrini, L. Paolini, S. Busatto and A. Radeghieri, *Front. Bioeng. Biotechnol.*, 2020, **7**, 1–10.